# Recoil-$\alpha$-fission and recoil-$\alpha$-$\alpha$-fission events observed in the reaction $^{48}$Ca+$^{243}$Am

U. Forsberg,[1] D. Rudolph,[1] L.-L. Andersson,[2] A. Di Nitto,[3] Ch.E. Düllmann,[2,3,4] J.M. Gates,[5] P. Golubev,[1] K.E. Gregorich,[5] C.J. Gross,[6] R.-D. Herzberg,[7] F.P. Heßberger,[2,4] J. Khuyagbaatar,[2] J.V. Kratz,[3] K. Rykaczewski,[6] L.G. Sarmiento,[1] M. Schädel,[4,8] A. Yakushev,[4] S. Åberg,[1] D. Ackermann,[4] M. Block,[4] H. Brand,[4] B.G. Carlsson,[1] D. Cox,[7] X. Derkx,[2,3] J. Dobaczewski,[9] K. Eberhardt,[2,3] J. Even,[2] C. Fahlander,[1] J. Gerl,[4] E. Jäger,[4] B. Kindler,[4] J. Krier,[4] I. Kojouharov,[4] N. Kurz,[4] B. Lommel,[4] A. Mistry,[7] C. Mokry,[2,3] W. Nazarewicz,[6,9,10] H. Nitsche,[5] J.P. Omtvedt,[11] P. Papadakis,[7] I. Ragnarsson,[1] J. Runke,[4] H. Schaffner,[4] B. Schausten,[4] Yue Shi,[6,10] P. Thörle-Pospiech,[2,3] T. Torres,[4] T. Traut,[3] N. Trautmann,[3] A. Türler,[12] A. Ward,[7] D.E. Ward,[1] N. Wiehl,[2,3]

[1] *Lund University, 22100 Lund, Sweden*
[2] *Helmholtz Institute Mainz, 55099 Mainz, Germany*
[3] *Johannes Gutenberg-Universität Mainz, 55099 Mainz, Germany*
[4] *GSI Helmholtzzentrum für Schwerionenforschung GmbH, 64291 Darmstadt, Germany*
[5] *Lawrence Berkeley National Laboratory, Berkeley, California 94720, USA*
[6] *Oak Ridge National Laboratory, Oak Ridge, Tennessee 37831, USA*
[7] *University of Liverpool, Liverpool L69 7ZE, United Kingdom*
[8] *Advanced Science Research Center, Japan Atomic Energy Agency, Tokai, Ibaraki 319-1195, Japan*
[9] *University of Warsaw, 00681 Warsaw, Poland*
[10] *University of Tennessee, Knoxville, Tennessee 37996, USA*
[11] *University of Oslo, 0315 Oslo, Norway and*
[12] *Paul Scherrer Institute and University of Bern, 5232 Villigen, Switzerland*

(Dated: March 4, 2022)

Products of the fusion-evaporation reaction $^{48}$Ca + $^{243}$Am were studied with the TASISpec set-up at the gas-filled separator TASCA at the GSI Helmholtzzentrum für Schwerionenforschung. Amongst the detected thirty correlated $\alpha$-decay chains associated with the production of element $Z = 115$, two recoil-$\alpha$-fission and five recoil-$\alpha$-$\alpha$-fission events were observed. The latter are similar to four such events reported from experiments performed at the Dubna gas-filled separator. Contrary to their interpretation, we propose an alternative view, namely to assign eight of these eleven decay chains of recoil-$\alpha$(-$\alpha$)-fission type to start from the $3n$-evaporation channel $^{288}$115. The other three decay chains remain viable candidates for the $2n$-evaporation channel $^{289}$115.

PACS numbers: 21.10.-k,23.20.Lv,23.60+e,27.90.+b

arXiv:1502.03030v1 [nucl-ex] 10 Feb 2015

In the quest for enhanced nuclear stability in the region of superheavy elements (SHE) – frequently defined as those with $Z \geq 104$ – the two elements flerovium (Fl, $Z = 114$) and livermorium (Lv, $Z = 116$) have recently been officially approved [1]. The interpretation of data on odd-$Z$ elements, however, is more challenging, while the study of nuclei with odd numbers of nucleons can be especially rewarding: The extra hindrance and thus delay for spontaneous fission (SF) renders other decay modes such as $\alpha$ decay and electron capture (EC) even more likely. Consequently, odd-$Z$ nuclei potentially give rise to decay chains with more $\alpha$-decay members than even-$Z$ ones. Additionally, $\alpha$ decay of odd-$A$ or odd-odd nuclei most often proceeds into excited states in the daughter nucleus, because unpaired nucleons typically tend to remain in the same single-particle orbitals as in the $\alpha$-decay parent [2, 3]. Observation of electromagnetic decays from these excited states can thus elucidate the low-lying nuclear structure of the daughter [4]. Such experimental studies have recently reached decay chains of element $Z = 115$ [5], while observations of odd-$Z$ elements beyond Rg have been reported up to $Z = 117$. See, e.g., Refs. [6–12] and references therein.

The expected complex nuclear structure of odd-$Z$ nuclei of SHE can easily translate into complex $\alpha$-decay sequences. Interestingly, however, for the description of many of the hitherto published $Z \geq 113$ decay chains it appears to suffice with just one type of $\alpha$-decay sequence per isotope, be it $^{278}$113 [12], $^{287-289}$115 [9], or $^{293,294}$117 [10, 11] (see also references therein). This simple but surprising picture might be due to limited statistics, combined with possibly comparable decay energies and half lives of different decay branches of a given isotope.

In this paper, new data on recoil-$\alpha$-($\alpha$)-SF events stemming from element $Z = 115$ are presented. A comprehensive assessment including corresponding data from Ref. [9] implies more complex decay sequences of $^{288,289}$115 than presented in previous reports on these isotopes [8, 9, 13]. It is demonstrated that the plain length of an $\alpha$-decay chain is not necessarily a good descriptor to define the reaction channel.

The Universal Linear Accelerator (UNILAC) at the GSI Helmholtzzentrum für Schwerionenforschung, Darmstadt, Germany, provided a $^{48}Ca^{8+}$ heavy-ion beam with a typical intensity of $6 \times 10^{12}$ ions per second, averaged over the pulsed structure of the UNILAC (5 ms beam on and 15 ms beam off). The experiment was conducted at two beam energies: Beam integrals of 2.13(12) and $3.89(23) \times 10^{18}$ $^{48}$Ca ions were collected at 5.400 and 5.462 MeV/u, respectively.

At the entrance of the recoil separator TASCA [14–16] the beam particles hit one out of four target segments, which were mounted on a rotating target wheel [17]. The thicknesses of these segments averaged to 0.83(1) mg/cm$^2$ $^{243}Am_2O_3$. The $^{243}$Am material originated from the Oak Ridge National Laboratory. At Mainz University, the $^{243}$Am was electroplated onto 2.20(5) $\mu$m thick titanium backing foils [18]. The $^{48}$Ca beam first had to pass through these foils. Estimates for the energy-loss of $^{48}$Ca ions in titanium and $^{243}Am_2O_3$ lead to mid-target beam energies of 242.1 and 245.0 MeV [19]. Based on the Myers-Swiatecki mass table [20], these laboratory energies convert into compound nucleus excitation energies of $E^* = 32.4$-$37.9$ MeV and 34.8-40.3 MeV across the target layers.

TASCA, filled with He-gas at $p_{\rm He} = 0.8$ mbar [21], was used in its so-called high-transmission mode and set to center ions with a magnetic rigidity of $B\rho = 2.21$ Tm in the focal plane for the major part of the experiment [22]. The multi-coincidence spectroscopy set-up TASISpec [23] was placed in TASCA's focal plane. The efficiency for transmitting element $Z = 115$ fusion-evaporation residues through TASCA and into TASISpec amounts to 30(3)% [22, 24].

Five 32 × 32-strip double-sided silicon strip detectors (DSSSD) form the heart of TASISpec. The ions passing TASCA are implanted in one of 1024 pixels of the downstream DSSSD, which is 6 × 6 cm$^2$ in area and 0.52 mm thick. Four additional DSSSDs of the same size but 1.0 mm thick are placed upstream. They are sensitive to charged-particle decay radiation emitted from the implanted ions into the backward hemisphere. Detector strips of these four DSSSDs were paired together electrically, i.e., they are handled effectively as 16 × 16-strip DSSSDs giving rise to another 1024 pixels. To detect photons coincident with charged-particle decays registered by the DSSSDs, five large, composite germanium detectors were placed closely behind each of the five DSSSDs [23].

The 96 preamplified signals [25] from the $n$-doped sides of the DSSSDs were recorded based on standard analog electronics [23]. The preamplified signals of the $p$-doped sides were digitized as 70-$\mu$s long traces by 60 MHz, 12-bit sampling ADCs [26]. The signals of the germanium detectors were handled by commercial 100-MHz, 16-bit sampling ADCs. The data acquisition was triggered by a coincident signal from a $p$-side and $n$-side strip of the implantation detector. The latter limits the energy threshold of the trigger to some 400 keV deposited. This is a condition, which is in practice always fulfilled by 10 MeV $\alpha$-decays. Time-averaged (cf. pulsed UNILAC beam structure) trigger rates were typically 100-120 events per second. Beam on-off status and irradiated target segment number were recorded as well. The data acquisition system also provided the possibility to send a signal to the UNILAC control system to switch off the primary $^{48}$Ca beam upon detection of an 8.5-11.0-MeV particle in one of the $n$-side strips of the implantation DSSSD during UNILAC beam-off periods. The beam was then chopped within 20 $\mu$s for periods of 5-60 seconds [5].

Si- and Ge-detector calibrations were performed using various radioactive sources in conjunction with precision pulser signals. During the offline data analysis, the calibrations were cross-checked with known $\alpha$-decay as well as $\gamma$-ray energies of background radiation mainly from transfer reaction products reaching the TASISpec implantation detector. More details on the detector set-up, electronics, data storage, and data analysis can be found in Refs. [5, 27–30].

As outlined in Ref. [5], a search for time- and position-correlated recoil-$\alpha$-$\alpha$, recoil-$\alpha$-SF, and recoil-SF sequences was conducted using

- $11.5 < E_{\rm rec} < 18.0$ MeV, beam on;
- $9.0 < E_{\alpha1} < 12.0$ MeV, $\Delta t_{\rm rec-\alpha1} = 5$ s, beam off, or $10.0 < E_{\alpha1} < 12.0$ MeV, $\Delta t_{\rm rec-\alpha1} = 1$ s, beam on;
- $9.0 < E_{\alpha2} < 11.0$ MeV, $\Delta t_{\alpha1-\alpha2} = 20$ s, beam off, or $9.5 < E_{\alpha2} < 11.0$ MeV, $\Delta t_{\alpha1-\alpha2} = 5$ s, beam on;
- $E_{\rm SF} > 120$ MeV, $\Delta t_{\alpha1-\rm SF} = 30$ s, beam off.

During beam-off and background measurement periods, only 64 fission events were recorded in total. Most of these were correlated with one of the thirty $\alpha$-decay chains, or could be associated with short-lived recoil-SF events of transfer reaction products such as $^{242m}$Am.

The thirty identified chains associated with the production of element 115 contain 23 five-$\alpha$ long chains. The spectroscopic results on these have been communicated in Ref. [5], further described in Refs. [28, 29], and are to be detailed in a forthcoming publication [30]. One of those 23 long chains was assigned to originate from the isotope $^{287}$115, and 22 from $^{288}$115 [5]. The combined data of these 22 decay chains and 31 corresponding ones from Ref. [9] are shown at the bottom of Fig. 1. The black histograms in Fig. 1 are the experimental spectra. In panels (a)-(c), the number of correlation times available to derive the half-life, $T_{1/2}$, of a given decay step is 47, 46, and 47, respectively. The expected time distributions for the corresponding half-lives are indicated by the shaded areas. In Figs. 1(d) and (e) the shaded areas relate to Geant4 Monte-Carlo simulations [32, 33], which are based on decay schemes suggested in Refs. [5, 28, 29, 33]. In short, one or several $\alpha$ decays populate excited states in the daughter nucleus. The excited states decay primarily via internal conversion. Energy summing of a detected $\alpha$ particle and one or more registered conversion or Auger electrons readily explains the relatively broad energy distributions observed.

To assess whether distributions of experimental correlation times are compatible with the assumption that each step can be described by one single half-life, a relatively "new test for random events of an exponential distribution" [34] was applied to the 53 chains. This is done (*i*) for the full data set, and (*ii*) subdivided into six data sets corresponding to the six different $^{48}$Ca beam energies exploited in Refs. [5, 9]. The result of this test can be found in Table IV and Fig. 4 of the Supplemen-

tal Material (SM) [31]. There is no clear hint towards the need of assuming the decay of more than one radioactive species for any of the decay steps of these 53 chains, thereby concurring with previous interpretations [9, 28, 29]. Therefore, and this is the most relevant result in the context of the present work, they serve as reference for the $3n$ evaporation channel $^{288}115$.

The focus lies now on the interpretation of two recoil-$\alpha$-SF (denoted C1,C2) and five recoil-$\alpha$-$\alpha$-SF (C3-C7) events from the present work, and four similar recoil-$\alpha$-$\alpha$-SF chains published by Oganessian *et al.* (D1-D4) [9]. Three decay scenarios are illustrated in Fig. 2 and discussed below: In 'scenario 1', all eleven recoil-$\alpha$(-$\alpha$)-SF chains are associated with $^{289}115$, with chain D3 forming a distinctively different sequence. In 'scenario 2', all recoil-$\alpha$-($\alpha$)-SF chains but D3 are considered to originate from $^{288}115$. For 'scenario 3', two chains, C4 and D4, are moved from $^{288}115$ to $^{289}115$, forming a decay sequence parallel to chain D3. On purpose, we refrain from using decay data suggested to originate from $^{293}117$ [6, 8, 10, 35]. Presence of links between decay chains associated with elements 115 and 117 are neither questioned nor subject of the present work.

The experimental results of the eleven recoil-$\alpha$(-$\alpha$)-SF chains are summarized in Table I. The number of chains of a given type expected to arise from random background in the whole implantation DSSSD, $N_{\rm random}$, is calculated according to Ref. [36]. Here, escape events relate to energies up to 4 MeV in a DSSSD pixel, while 9-11 MeV is set for full energy and reconstructed events. The time periods used in the calculations are 2 s, 10 s, and 50 s for decay steps one, two, and three. These correspond to roughly ten times the respective average half-lives of the scenarios (cf. Fig. 1). Count rates per pixel are determined in the two pre-defined energy ranges separately for beam-on and beam-off periods. Essentially, the non-random origins of TASISpec chains C1-C7 are defined by the overall small number of fission events observed during beam-off periods, in combination with the rather short time periods, $\Delta t$, between the detected recoil implantation and subsequent fission events.

The individual correlation times and decay energies of the eleven recoil-$\alpha$-($\alpha$)-SF chains are also provided in Fig. 1(a)-(e), labeled with C1-C7 and D1-D4, respectively. At first glance, there seems to be very little if any difference in the distribution of these data points compared with the suggested reference distributions of the 53 five-$\alpha$ long chains associated with $^{288}115$ (see above). Interestingly, none of the previous publications on decay chains associated with elements 115 and 117 (see, e.g., Refs. [7–10, 35] dwells on this obvious similarity. Instead, it has essentially been argued that the length of a decay chain is a sufficient descriptor of its origin: For example, all five-$\alpha$ long chains observed at low excitation energies of the compound nucleus $^{291}115$, $E^* < 37$ MeV, were associated with the decay of the $3n$ evaporation channel $^{288}115$, whilst chains D1-D4 were interpreted to originate from the $2n$ evaporation channel $^{289}115$ [9].

Columns 2 ('$3n$') and 3 (C1-C7, D1-D4) of Table II provide the half-life analyses of correlation times. This very simple decay scenario, essentially based on the observed length of a decay chain, implies a ratio of maximum production cross-sections $R_\sigma = \sigma(2n)/\sigma(3n) \approx 0.5$ (cf. Ref. [9] and Table III). Such high relative or absolute yields of the production of the $2n$ reaction channel $^{289}115$ are not necessarily consistent with expectations from nuclear reaction theory [37, 38]. Systematic studies of fusion-evaporation reactions leading to heavy or superheavy nuclei [39] also prefer $R_\sigma \lesssim 10\%$. Secondly, a closer look at Fig. 1 suggests that chain D3 is neither compatible with the $3n$ reference values nor the average of the remaining ten recoil-$\alpha$-($\alpha$)-SF events (cf. column 4 of Table II): all three decay times of D3 reach significantly beyond the upper limit of the respective reference time distribution. Its energy $E_2$ is also significantly lower than that of all other chains. While a single extreme value would not pose a statistical problem, the fact that in chain D3 four out of five observables differ significantly from the expectations does.

This observation is turned into a more robust figure-of-merit (FoM). It provides a measure for the congruence of the time sequence of the first decay steps of a single (element 115) chain with respect to the average of a certain 'reference' ensemble of (element 115) chains. For each of the decay steps, $i = 1, 2, 3$, the value $P_i$ is the reference probability density function for correlation times in logarithmic-sized bins (see Ref. [34]) evaluated for the measured correlation time. Thereafter, it is normalised with the constant $e$ such that the values range from 0 to 1. Figure 1 shows the form of the functions, here normalised to the amount of data. To account for the uncertainties in the reference half-lives, $P_i$ is given the value 1 whenever the correlation time is within the confidence limits. If it is above (below) the confidence interval, the upper (lower) limit is used. To be able to compare chains with differing numbers, $n$, of decay steps, the FoM=$\langle P_t \rangle = \sqrt[n]{\prod P_i}$ is calculated as the geometric average. Deviations in decay energy only serve as supportive argument, since the comprehensive data of element 115 decay chains rather suggests a range of energies than distinct peaks for decay steps 115 → 113 and 113 → Rg [5, 29].

The rightmost columns in Table I list $\langle P_t \rangle$ for the three decay scenarios proposed in Fig. 2. For more detailed statistical assessments see Tables SM VI-X. In short, $\langle P_t \rangle \gtrsim 50\%$ appears to be a solid *indicator* for congruence. In turn, $\langle P_t \rangle \lesssim 25\%$ *signals* a decay chain different from the reference.

'Scenario 1', cf. Fig. 2(a):
Outstandingly low values of $\langle P_t \rangle$(D3)=0.10%, 18%, and 0.074% are obtained for chain D3 when cross-checked versus the 53 five-$\alpha$-long chains, the average of all eleven, or the remaining ten recoil-$\alpha$-($\alpha$)-SF chains, respectively (cf. Tables I and SM VI-VIII). The conclusion is that chain D3 is not compatible with any subset of the other element 115 decay chains. D3 thus represents a single but distinct decay sequence starting from a given state

of a certain isotope of element 115. Note that it is *not* the intention to question the existence of this chain as such. In fact, according to our interpretations, D3 remains a valid candidate to be attributed to $^{289}$115 (see below).

Note also that the decay times of D3 are similar to the chain $^{289}$Fl→$^{285}$Cn→$^{281}$Ds [7, 16, 40]. This decay sequence can in principle be entered by EC decay of $^{289}$115 or $^{285}$113. However, both $\alpha$-decay energies measured for D3 differ distinctively from the ones expected for the mentioned even-$Z$ chain. Therefore, this explanation for D3 is disregarded.

'Scenario 2', cf. Fig. 2(b):
In decay 'scenario 2', all the other ten recoil-$\alpha$-($\alpha$)-SF chains – C1-C7, D1, D2, and D4 – are considered to start from the isotope $^{288}$115. Comparing columns 2 and 4 in Table II and inspecting Fig. 2(a), the correlation time analysis indicates essentially compatible half-lives for all three decay steps. There is no significant FoM difference between the congruence test of these ten chains among themselves ($\langle$FoM$\rangle$ = 64%) and the values obtained when they are associated with decays of $^{288}$115 ($\langle$FoM$\rangle$ = 65%). There is, however, a clear improvement compared with plain averages of all eleven recoil-$\alpha$-($\alpha$)-SF chains ($\langle$FoM$\rangle$ = 52%, cf. Tables SM VII-IX).

The assignment of the ten chains to $^{288}$115 implies, at first sight, SF branching ratios of $b_{\rm SF} = 2/63 = 3.2\%$ for $^{284}$113 and $b_{\rm SF} = 8/61 = 13\%$ for $^{280}$Rg, respectively. It is important to note, however, that none of the experiments has been sensitive to EC decay. Hence, other options are EC decay branches of $^{284}$113 or $^{280}$Rg into even-even $^{284}$Cn or $^{280}$Ds. The latter are either known (see, e.g., Refs. [7, 16, 40]) or expected (see, e.g., Refs. [41–43]) to decay with $T_{1/2}$(SF)$\ll$ 1 s. In this scenario, partial SF or EC half-lives amount to about 30 s for both $^{284}$113 and $^{280}$Rg. This suggests SF hindrance factors of 300 relative to $^{284}$Cn. This value is rather low for odd-odd nuclei, because hindrance is expected from each of the two unpaired nucleons. Already for one unpaired nucleon, hindrance factors are typically above 1000 [44, 45]. Thus, we rather suggest EC preceding SF of the respective even-even daughter. The observation of SF or EC branches in this region of the nuclear chart is consistent with recent theoretical estimates [46, 47] (see especially Figs. 4 and 6 in Ref. [46]). For the half-life analysis in Table II and Table SM V, SF of $^{284}$113 and $^{280}$Rg has been assumed, i.e., the short finite lifetime of a potential EC daughter has not been considered.

'Scenario 3', cf. Fig. 2(c):
Further examinations of Fig. 1 and Tables SM VII-IX reveal that C4 and D4 may have a common origin, which is different from that of all other chains: $\langle P_t\rangle < 25\%$ for both C4 and D4 in all hitherto discussed combinations, and in particular $E_2$ of chain D4 lies outside the typical window for $\alpha$-decay energies of $^{284}$113. The rather short correlation time of the observed fission event of chain D4 is also striking. Columns 5 and 6 of Table II provide the half-lives resulting from the correlation-time analysis of the remaining eight chains – C1-C3, C5-C7, D1-D2 – and C4 combined with D4, respectively.

The numbers in Table II indicate that there is no obvious reason *not* to assign the former eight chains with either SF or EC decay branches of decay chains starting with $^{288}$115. Chains C4 and D4 *may* form a second decay sequence starting from $^{289}$115, parallel to chain D3. It is consistent with – but not conditioned by – the detection of C4 at the lower beam energy of the present TASISpec experiment. Despite significant differences of the first decay steps of C4 and D4 we *propose* them to stem from the same level. Combining these two chains is the simplest approach within the available statistics ($\langle$FoM$\rangle$ = 74%, cf. Table SM X). A related scenario could include also chain D1 into this subset, in this case based on a selection according to decay energy of the first decay step.

Table III provides measured cross sections for the three decay scenarios shown in Fig. 2. For 'scenario 1' the numbers would be consistent with Fig. 4 of Ref. [9], but it implies too high values for the 2$n$ channel (see above). In the preferred 'scenario 3', the cross-section of the 2$n$ reaction channel $^{289}$115 amounts to $\approx$ 1 pb at low excitation energies $E^* \approx 34$ MeV. This corresponds to $\approx 10\%$ of the maximum cross-section of the 3$n$-channel around $E^* = 37$ MeV and is in line with theoretical expectations.

Figure 3 provides proton single-particle energies predicted by macroscopic-microscopic model parametrisations [48–50] and a Skyrme energy density functional [51–53]. Independent of the model or the parametrisation, the nuclear shape is predicted to change from near-sphericity towards prolate deformation along the decay chain $^{289}$115→$^{285}$113 →$^{281}$Rg. Most interestingly, however, all models suggest the same decay *pattern*, namely two independent $\alpha$-decay chains: Exemplified by Fig. 3(b), once $^{289}$115 is created as final fusion-evaporation product, excited states will decay by electromagnetic radiation into *either* a high-$\Omega$ positive-parity state (here: [606]13/2) *or* a low-$\Omega$ negative-parity state (here: [541]1/2). The two families (high-$\Omega$ and low-$\Omega$) of Nilsson orbitals remain separate for the daughter $^{285}$113 and grand-daughter $^{281}$Rg, giving rise to two parallel $\alpha$-decay sequences. The detailed predictions are highly model dependent and it is currently not possible to say which predicted decay sequence can be associated with the observed ones.

In summary, seven new recoil-$\alpha$-($\alpha$)-SF events were observed following the fusion-evaporation reaction $^{48}$Ca+$^{243}$Am. An assessment of these seven together with four previously published [9] decay chains suggests a revised decay scenario of isotopes of element 115: Eight of these eleven decay chains are interpreted to originate from $^{288}$115. They represent either SF or EC decay branches of $^{284}$113 and $^{280}$Rg. The remaining three chains can account for two separate decay sequences of the isotope $^{289}$115. Two parallel sequences are readily explained by a set of nuclear structure models. Clearly, more high-quality spectroscopic data near the barrier of the $^{48}$Ca+$^{243}$Am reaction is needed to verify *any proposed* decay scenario of $^{288,289}$115. This is also consid-

ered necessary to establish statistically firm links towards $^{293}117$. A comprehensive discussion of this subject is beyond the scope of the present paper.

The authors would like to thank the ion-source and the accelerator staff at GSI. This work is supported by the European Community FP7 – Capacities ENSAR No. 262010, the Royal Physiographic Society in Lund, the Euroball Owners Committee, the Swedish Research Council, the German BMBF, the Office of Nuclear Physics, U.S. Department of Energy, and the UK Science and Technology Facilities Council.

[1] R.C. Barber, P.J. Karol, H. Nakahara, E. Vardaci, and E. Vogt, Pure Appl. Chem. **83** (7), 1485 (2011).
[2] A. Bohr and B.R. Mottelson, *Nuclear Structure Volume II*, (W. A. Benjamin, Inc., Massachusetts, 1975).
[3] G.T. Seaborg and W.D. Loveland, *The Elements Beyond Uranium*, (Wiley-Interscience, New York, 1990).
[4] R.-D. Herzberg and P.T. Greenlees, Prog. Part. Nucl. Phys. **61**, 674 (2008).
[5] D. Rudolph *et al.*, Phys. Rev. Lett. **111**, 112502 (2013).
[6] Yu. Ts. Oganessian *et al.*, Phys. Rev. Lett. **104**, 142502 (2010).
[7] Yu. Ts. Oganessian, Radiochim. Acta **99**, 429 (2011).
[8] Yu. Ts. Oganessian *et al.*, Phys. Rev. Lett. **108**, 022502 (2012).
[9] Yu. Ts. Oganessian *et al.*, Phys. Rev. C **87**, 014302 (2013).
[10] Yu. Ts. Oganessian *et al.*, Phys. Rev. C **87**, 054621 (2013).
[11] J. Khuyagbaatar *et al.*, Phys. Rev. Lett. **112**, 172501 (2014).
[12] K. Morita *et al.*, J. Phys. Soc. Jpn. **81** 103201 (2012).
[13] Yu. Ts. Oganessian *et al.*, Phys. Rev. C **69**, 021601(R) (2004).
[14] M. Schädel, Eur. Phys. J. D **45**, 67 (2007).
[15] A. Semchenkov *et al.*, Nucl. Instr. Meth. **B266**, 4153 (2008).
[16] J.M. Gates *et al.*, Phys. Rev. C **83**, 054618 (2011).
[17] E. Jäger, Ch.E. Düllmann, J. Khuyagbaatar, J. Krier, M. Schädel, T. Torres, and A. Yakushev, J. Radioanal. Nucl. Chem. **299**, 1073 (2014).
[18] J. Runke *et al.*, J. Radioanal. Nucl. Chem. **299**, 1081 (2014).
[19] J.F. Ziegler, Nucl. Instr. Meth. **A219**, 1024 (2004).
[20] W.D. Myers and W.J. Swiatecki, Nucl. Phys. **A601**, 141 (1996).
[21] J. Khuyagbaatar *et al.*, Nucl. Instr. Meth. **A689**, 40 (2012).
[22] U. Forsberg *et al.*, Acta Phys. Pol. **43**, 305 (2012).
[23] L.-L. Andersson *et al.*, Nucl. Instr. Meth. **A622**, 164 (2010).
[24] K.E. Gregorich, Nucl. Instr. Meth. **A711**, 47 (2013).
[25] P. Golubev *et al.*, Nucl. Instrum. Meth. **A723**, 55 (2013).
[26] J. Hoffmann *et al.*, GSI Scientific Report 2011, GSI Report 2012-1 (2012).
[27] U. Forsberg *et al.*, Eur. Phys. J. Web of Conferences **66**, 02036 (2014).
[28] D. Rudolph *et al.*, Acta Phys. Pol. **B45**, 263 (2014).
[29] D. Rudolph *et al.*, J. Rad. Nucl. Chem., (2014) DOI 10.1007/s10967-014-3445-y .
[30] U. Forsberg *et al.*, to be published.
[31] See Supplemental Material at http://link.aps.org .
[32] L.G. Sarmiento, L.-L. Andersson, D. Rudolph, Nucl. Instr. Meth. **A667**, 26 (2012).
[33] L.G. Sarmiento *et al.*, Proc. 10th Latin American Symposium on Nuclear Physics and Applications, PoS(X LASNPA)057 (2014).
[34] K.-H. Schmidt, Eur. Phys. J. A **8**, 141 (2000).
[35] Yu. Ts. Oganessian *et al.*, Phys. Rev. C **83**, 054315 (2011).
[36] K.-H. Schmidt, C.-C. Sahm, K. Pielenz, and H.-G. Clerc, Z. Phys. A **316**, 19 (1984).
[37] V.I. Zagrebaev, Nucl. Phys. **A734**, 164 (2004).
[38] K. Siwek-Wilczyńska, T. Cap, M. Kowal, A. Sobiczewski, and J. Wilczyński, Phys. Rev. C **86**, 014611 (2012).
[39] W. Reisdorf and M. Schädel, Z. Phys. A **343**, 47 (1992).
[40] Ch.E. Düllmann *et al.*, Phys. Rev. Lett. **104**, 252701 (2010).
[41] R. Smolańczuk, J. Skalski and A. Sobiczewski, Phys. Rev. C **52**, 1871 (1995).
[42] M. Warda and J.L. Egido, Phys. Rev. C **86**, 014322 (2012).
[43] A. Staszczak, A. Baran, and W. Nazarewicz, Phys. Rev. C **87**, 024320 (2013).
[44] D.C. Hoffman and M.R. Lane, Radiochim. Acta **70/71**, 135 (1995).
[45] F.P. Heßberger, Eur. Phys. J. Web of Conferences **66**, 02048 (2014).
[46] A.V. Karpov, V.I. Zagrebaev, Y. Martinez Palenzuela, L. Felipe Ruiz, and W. Greiner, Int. J. Mod. Phys. **E21**, 1250013 (2012).
[47] V. Zagrebaev, A. Karpov, and W. Greiner, J. Phys.: Conf. Ser. **420**, 012001 (2013); Acta Phys. Pol. **45**, 291 (2014).
[48] B.G. Carlsson and I. Ragnarsson, Phys. Rev. C **74**, 011302 (2006).
[49] S.G. Nilsson, C.F. Tsang, A. Sobiczewski, Z. Szymański, S. Wycech, C. Gustafson, I.-L. Lamm, P. Möller, and B. Nilsson, Nucl. Phys. A **131**, 1 (1969).
[50] A. Parkhomenko and A. Sobiczewski, Acta Phys. Pol. **B35**, 2447 (2004).
[51] S. Ćwiok, W. Nazarewicz, and P.H. Heenen, Phys. Rev. Lett. **83**, 1108 (1999).
[52] M. Kortelainen, J. McDonnell, W. Nazarewicz, P.-G. Reinhard, J. Sarich, N. Schunck, M.V. Stoitsov, and S.M. Wild, Phys. Rev. C **85**, 024304 (2012).
[53] Yue Shi, D.E. Ward, B.G. Carlsson, J. Dobaczewski, W. Nazarewicz, I. Ragnarsson, and D. Rudolph, Phys. Rev. C **90**, 014308 (2014).

TABLE I. Mid-target laboratory-frame beam energies, energies of the implanted recoils $E_{\rm rec}$, decay energies $E_1$, $E_2$ and $E_3$, together with the associated correlation times of recoil-$\alpha$-SF and recoil-$\alpha$-$\alpha$-SF decay chains observed in the $^{48}$Ca+$^{243}$Am reaction. Entries in bold were recorded during beam-off periods. The number of $\gamma$ rays detected in prompt coincidence with SF events, $N_\gamma$(SF), are also specified. $N_{\rm random}$ corresponds to the number of chains of a given type expected to arise from random background [36]. $\langle P_t \rangle$ represents a figure-of-merit for the congruence of a single chain with a proposed decay scenario. See text, Fig. 2, and Supplemental Material for details. The decay characteristics of the four chains listed in Table III in Ref. [9] are included for completeness, denoted D1-D4.

| No. | $\langle E_{\rm lab} \rangle$ (MeV) | $E_{\rm rec}$ (MeV) pixel (x,y) | $E_1$ (MeV) $\Delta t_1$ (s) | $E_2$ (MeV) $\Delta t_2$ (s) | $E_3$ (MeV) $\Delta t_3$ (s) | $N_\gamma$(SF) | $N_{\rm random}$ | $\langle P_t \rangle$ for scenario[d] 1 | 2 | 3 |
|---|---|---|---|---|---|---|---|---|---|---|
| C1 | 245.0 | 12.3 | **10.51(1)** | **242**[a] | | **6** | $< 2 \cdot 10^{-5}$ | 91 | 81 | 80 |
| | | 268 (8,12) | **0.227** | **0.378** | | | | | | |
| C2 | 242.1 | 16.2 | **1.45(1)**[b] | **211** | | **> 4** | $< 6 \cdot 10^{-2}$ | 64 | 61 | 63 |
| | | 425 (13,9) | **0.0645** | **0.366** | | | | | | |
| C3 | 242.1 | 13.9 | 10.54(4)[c] | **9.95(5)**[c] | **196** | **8** | $< 2 \cdot 10^{-6}$ | 49 | 53 | 53 |
| | | 681 (21,9) | 0.261 | **1.15** | **0.343** | | | | | |
| C4 | 242.1 | 14.5 | 10.34(1) | **9.89(1)** | **218**[a] | **> 5** | $< 2 \cdot 10^{-6}$ | 19 | 11 | 74 |
| | | 344 (10,24) | 1.46 | **0.0262** | **0.432** | | | | | |
| C5 | 242.1 | 13.8 | **10.49(4)**[c] | **9.97(1)** | **135** | **9** | $< 3 \cdot 10^{-9}$ | 80 | 79 | 79 |
| | | 554 (17,10) | **0.345** | **0.369** | **14.4** | | | | | |
| C6 | 245.0 | 14.5 | **10.53(1)** | **9.89(5)**[c] | **230**[a] | **9** | $< 3 \cdot 10^{-9}$ | 97 | 100 | 100 |
| | | 205 (6,13) | **0.210** | **1.05** | **8.27** | | | | | |
| C7 | 245.0 | 11.9 | **0.541(3)**[b] | 3.12(1)[b] | **230**[a] | **> 4** | $< 1 \cdot 10^{-1}$ | 81 | 71 | 67 |
| | | 128 (4,0) | **0.815** | 2.33 | **2.89** | | | | | |
| D1 | 240.5 | 11.38 | 10.377(62) | **9.886(62)** | **215.7** | | | 82 | 87 | 87 |
| | | | 0.2562 | **1.4027** | **1.9775** | | | | | |
| D2 | 241.0 | 15.18 | 10.540(123)[c] | 9.916(72) | **214.9**[a] | | | 67 | 76 | 78 |
| | | | 0.0661 | 1.5500 | **2.3638** | | | | | |
| D3 | 241.0 | 9.04 | 10.373(50) | 9.579(50) | 141.1 | | | n/a | n/a | n/a |
| | | | 2.3507 | 22.5822 | 60.1855 | | | | | |
| D4 | 241.0 | 13.35 | 10.292(170)[c] | 10.178(55) | **182.2**[a] | | | 23 | 25 | 63 |
| | | | 0.0536 | 0.4671 | **0.0908** | | | | | |

[a]Fission event registered by both implantation and box detector.
[b]Escaped $\alpha$ particle registered solely by the implantation detector.
[c]Reconstructed energy of an $\alpha$ particle registered by both implantation and box detector.
[d]For details see Tables VII, IX and X of the Supplemental Material.

TABLE II. Half-lives, $T_{1/2}$, derived from the correlation times of decays of isotopes of $Z = 115$, $Z = 113$ and Rg. The column labeled '3$n$' relates to the reference decay chains associated with the 3$n$ reaction channel in Refs. [5, 9, 28]. The other columns describe different scenarios (cf. Fig. 2) of the decay data from recoil-$\alpha$-SF and recoil-$\alpha$-$\alpha$-SF events.

| data selection | 3$n$ [5, 9] | C1-C7 D1-D4 | C1-C7 D1,D2,D4 | C1-C3 C5-C7 D1,D2 | C4,D4 |
|---|---|---|---|---|---|
| | $T_{1/2}$ (s) | $T_{1/2}$ (s) | $T_{1/2}$ (s) | $T_{1/2}$ (s) | $T_{1/2}$ (s) |
| $Z = 115$ | $0.16(^{3}_{2})$ | $0.39(^{17}_{9})$ | $0.26(^{12}_{6})$ | $0.19(^{11}_{5})$ | $0.54(^{129}_{22})$ |
| $Z = 113$ | $0.92(^{16}_{12})$ | $2.0(^{9}_{5})$ | $0.63(^{29}_{15})$ | $0.75(^{41}_{20})$ | $0.17(^{42}_{7})$ |
| Rg | $4.8(^{8}_{6})$ | $7.0(^{35}_{18})$ | $2.7(^{15}_{7})$ | $3.5(^{24}_{10})$ | $0.19(^{46}_{8})$ |

TABLE III. Number of chains and production cross sections, $\sigma_{\rm prod}$, of $^{287-289}115$ derived for three decay scenarios (cf. Fig. 2) from the thirty decay chains observed in the TASISpec experiment (chains C1-C7 and 23 five-$\alpha$ long chains [5]). The observation of a single decay chain relates to a production cross section of $\sigma = 0.93(12)$ and 0.51(7) pb for mid-target beam energies 242.1 and 245.0 MeV, respectively. The systematic uncertainty accounts for uncertainties in beam integrals, target thickness, transport efficiency, and identification probability. Standard deviations of systematic uncertainties are given together with statistical uncertainties using a 68% confidence level [36].

| | | | scenario 1 | | scenario 2 | | scenario 3 | |
|---|---|---|---|---|---|---|---|---|
| $\langle E_{\rm lab}\rangle$ (MeV) | $E^*$ (MeV) [20] | reaction channel | no. of chains | $\sigma_{\rm prod}$ (pb) | no. of chains | $\sigma_{\rm prod}$ (pb) | no. of chains | $\sigma_{\rm prod}$ (pb) |
| 242.1 | 32.4-37.9 | $2n$ | 4 | $3.7 \pm 0.5^{+2.8}_{-1.9}$ | 0 | $< 1.9$ | 1 | $0.93 \pm 0.12^{+2.14}_{-0.77}$ |
| | | $3n$ | 8 | $7.5 \pm 1.0^{+3.6}_{-2.6}$ | 12 | $11.2 \pm 1.4^{+4.2}_{-3.2}$ | 11 | $10.3 \pm 1.3^{+4.0}_{-3.1}$ |
| | | $4n$ | 0 | $< 1.9$ | 0 | $< 1.9$ | 0 | $< 1.9$ |
| 245.0 | 34.8-40.3 | $2n$ | 3 | $1.5 \pm 0.2^{+1.4}_{-0.9}$ | 0 | $< 1.1$ | 0 | $< 1.1$ |
| | | $3n$ | 14 | $7.2 \pm 0.9^{+2.4}_{-1.9}$ | 17 | $8.7 \pm 1.1^{+2.6}_{-2.1}$ | 17 | $8.7 \pm 1.1^{+2.6}_{-2.1}$ |
| | | $4n$ | 1 | $0.51 \pm 0.07^{+1.17}_{-0.42}$ | 1 | $0.51 \pm 0.07^{+1.17}_{-0.42}$ | 1 | $0.51 \pm 0.07^{+1.17}_{-0.42}$ |

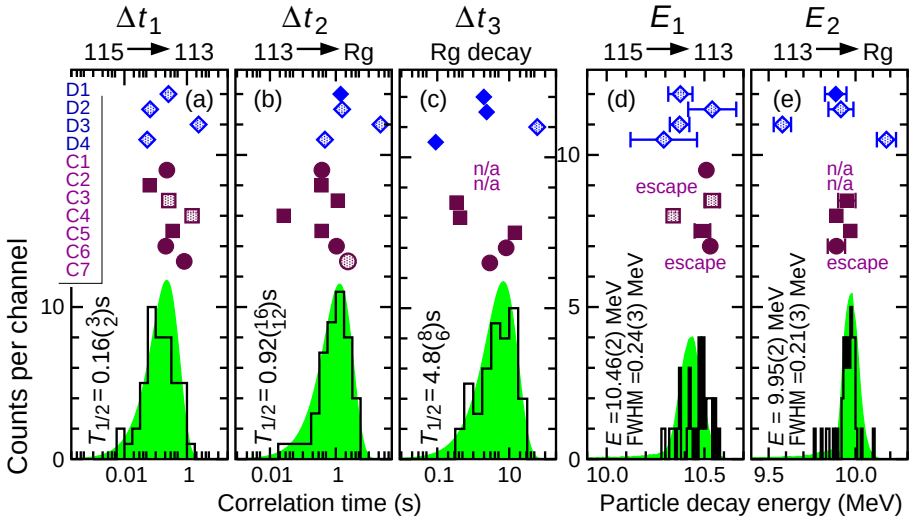



FIG. 1. (Color online) Correlation times [(a)-(c)] and particle decay-energy spectra [(d) and (e)] of decay chains observed in the reaction $^{48}$Ca+$^{243}$Am. The black histograms are reference spectra and relate to experimental data from the 53 chains associated with the $3n$ evaporation channel $^{288}115$ in Refs. [5, 9, 28]. The shaded areas in panels (a)-(c) are the corresponding time distributions. The shaded areas in panels (d) and (e) are the energy distributions derived from Monte Carlo simulations as outlined in Refs. [5, 29, 33]. The data points of the eleven observed recoil-$\alpha$-($\alpha$-)fission events are provided on top of each spectrum, labeled with an identifier according to Table I. Filled symbols indicate measurement during beam-off periods. Diamonds refer to data from Ref. [9], and squares and circles refer to the present data observed at 242.1 and 245.0 MeV mid-target beam energy, respectively. 'n/a' means 'not applicable', 'escape' denotes events with low-energy detection solely in the implantation DSSSD.

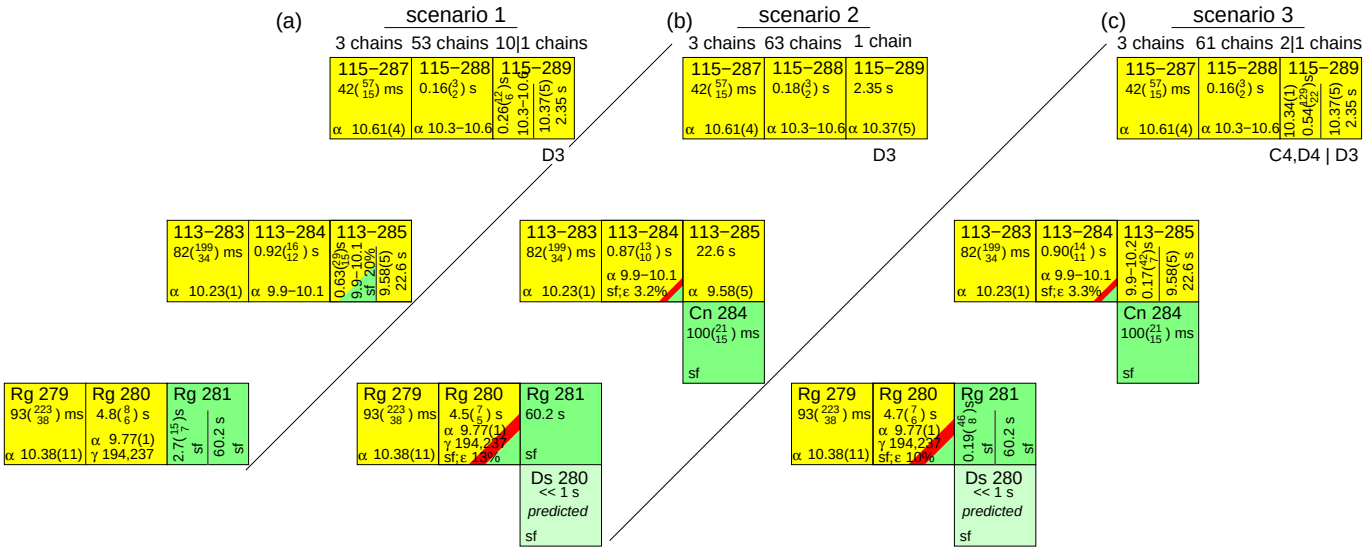



FIG. 2. (Color online) Three different decay scenarios of directly produced isotopes of element $Z = 115$ down to Rg, using previously published [5, 9] and present data. Half-lives, $T_{1/2}$, are provided with uncertainties. Particle-decay energies or ranges of decay energies are given in MeV, $\gamma$-ray energies in keV. See text for detailed discussions.

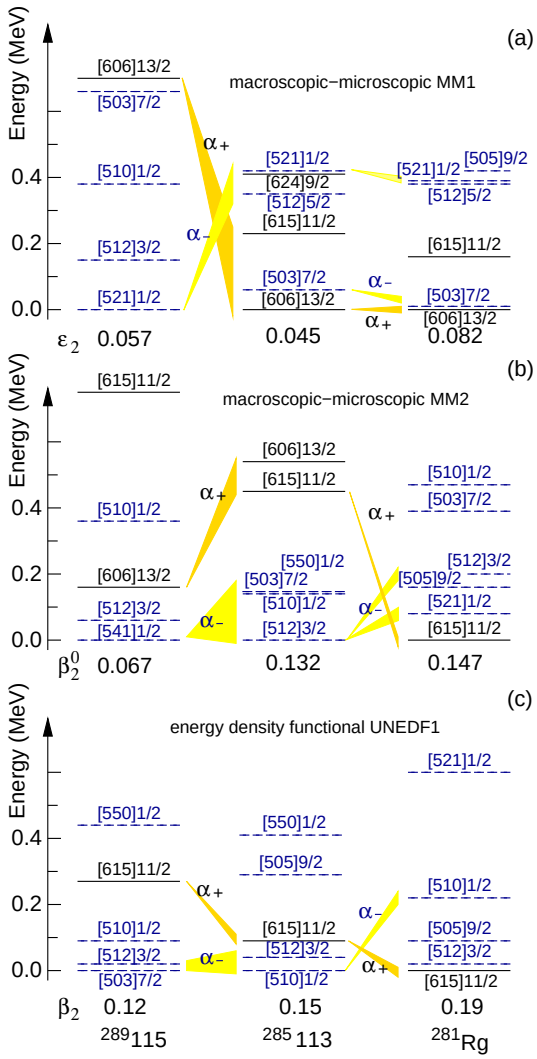



FIG. 3. (Color online) Nuclear structure predictions of low-lying states in $^{289}115$, $^{285}113$, and $^{281}$Rg. Panels (a) and (b) are based on two different macroscopic-microscopic approaches, MM1 [48, 49] and MM2 [50]. Panel (c) originates from the self-consistent Skyrme energy density functional UNEDF1 [52, 53]. The results from UNEDF1$^{\rm SO}$ are similar to MM2 [53]. Proton single-particle states are labeled with their asymptotic Nilsson quantum numbers $[Nn_z\Lambda]\Omega$. Full (black) lines represent positive-parity states, dashed (blue) lines negative-parity states. Selected $\alpha$-decay sequences among high-$\Omega$ positive-parity ($\alpha_+$) and low-$\Omega$ negative-parity ($\alpha_-$) states are indicated by shaded areas. $\epsilon_2$, $\beta_2^0$, $\beta_2$, respectively, denote predicted quadrupole deformations.

# Recoil-$\alpha$-fission and recoil-$\alpha$-$\alpha$-fission events observed in the reaction $^{48}$Ca+$^{243}$Am

U. Forsberg,[1] D. Rudolph,[1] L.-L. Andersson,[2] A. Di Nitto,[3] Ch.E. Düllmann,[2,3,4] J.M. Gates,[5] P. Golubev,[1] K.E. Gregorich,[5] C.J. Gross,[6] R.-D. Herzberg,[7] F.P. Heßberger,[2,4] J. Khuyagbaatar,[2] J.V. Kratz,[3] K. Rykaczewski,[6] L.G. Sarmiento,[1] M. Schädel,[4,8] A. Yakushev,[4] S. Åberg,[1] D. Ackermann,[4] M. Block,[4] H. Brand,[4] B.G. Carlsson,[1] D. Cox,[7] X. Derkx,[2,3] J. Dobaczewski,[9] K. Eberhardt,[2,3] J. Even,[2] C. Fahlander,[1] J. Gerl,[4] E. Jäger,[4] B. Kindler,[4] J. Krier,[4] I. Kojouharov,[4] N. Kurz,[4] B. Lommel,[4] A. Mistry,[7] C. Mokry,[2,3] W. Nazarewicz,[6,9,10] H. Nitsche,[5] J.P. Omtvedt,[11] P. Papadakis,[7] I. Ragnarsson,[1] J. Runke,[4] H. Schaffner,[4] B. Schausten,[4] Yue Shi,[6,10] P. Thörle-Pospiech,[2,3] T. Torres,[4] T. Traut,[3] N. Trautmann,[3] A. Türler,[12] A. Ward,[7] D.E. Ward,[1] N. Wiehl,[2,3]

[1] *Lund University, 22100 Lund, Sweden*
[2] *Helmholtz Institute Mainz, 55099 Mainz, Germany*
[3] *Johannes Gutenberg-Universität Mainz, 55099 Mainz, Germany*
[4] *GSI Helmholtzzentrum für Schwerionenforschung GmbH, 64291 Darmstadt, Germany*
[5] *Lawrence Berkeley National Laboratory, Berkeley, California 94720, USA*
[6] *Oak Ridge National Laboratory, Oak Ridge, Tennessee 37831, USA*
[7] *University of Liverpool, Liverpool L69 7ZE, United Kingdom*
[8] *Advanced Science Research Center, Japan Atomic Energy Agency, Tokai, Ibaraki 319-1195, Japan*
[9] *University of Warsaw, 00681 Warsaw, Poland*
[10] *University of Tennessee, Knoxville, Tennessee 37996, USA*
[11] *University of Oslo, 0315 Oslo, Norway and*
[12] *Paul Scherrer Institute and University of Bern, 5232 Villigen, Switzerland*

(Dated: March 4, 2022)

PACS numbers: 21.10.-k,23.20.Lv,23.60+e,27.90.+b

arXiv:1502.03030v1 [nucl-ex] 10 Feb 2015

This Supplemental Material contains one figure and six tables to support the arguments in the main article.

Figure SM 4 and Table SM IV provide a consistency check [34] of the 56 five-$\alpha$ long decay chains attributed to the decay of the $3n$ (53 chains) and $4n$ (3 chains) evaporation channel, $^{288}$115 and $^{287}$115, following the fusion-evaporation reaction $^{48}$Ca+$^{243}$Am at different beam energies and experiments [5, 9].

Table SM V is an extended version of Table II of the main article. It includes the results of the test proposed in Ref. [34] for different decay scenarios and subsets of decay chains associated with the eleven observed recoil-$\alpha$-($\alpha$)-chains, which are considered to stem from element $Z = 115$.

Tables SM VI-X provide the individual number of a probability check of the first three decay steps of all hitherto published 67 decay chains associated with element $Z = 115$; Table SM VI lists the complete comparison with respect to the anticipated reference of the 53 five-$\alpha$ long decay chains originating from $^{288}$115, while Tables SM VII-X relate to the different decay scenarios proposed and discussed in the main article.

TABLE IV. Overview of analyses according to Ref. [34] of 53 five-$\alpha$ chains associated with $^{288}115$ at different beam energies [5, 9]. The last column summarizes additional three chains associated with $^{287}115$. See Fig. SM 4 for an illustration.

| $\langle E_{\rm lab}\rangle$ (MeV) | 239.8 | 240.8 | 242.1 | 243.4 | 245.0 | 248.1 | ALL | 253.4 |
|---|---|---|---|---|---|---|---|---|
| $E^*$ [20] | 31.1-35.3 | 31.4-36.4 | 32.4-37.9 | 34.0-38.3 | 34.8-40.3 | 38.0-42.3 | | 42.4-47.2 |
| $d_{\rm target}$ (mg/cm$^2$) | 0.37 | 0.84;0.68 | 0.83(1) | 0.37 | 0.83(1) | 0.36;0.37 | | 0.36;0.68 |
| integral ($10^{18}$) | 11.7 | 10.4 | 2.13(12) | 3.3 | 3.89(23) | 4.3+3.7 | 39.4 | 4.3+4.4 |
| No. of chains | 7 | 12 | 8 | 6 | 14 | 3+3 | 53 | 1+1(+1)[a] |
| $\sigma_{\rm prod}$ (pb) | $3.5(^{27}_{15})$ | | $7.5(10)(^{36}_{26})$ | $8.5(^{64}_{37})$ | $7.2(9)(^{24}_{19})$ | $\sim 4$ | | $\sim 1$ |
| $T_{1/2}(^{288}115)$ (s) | $0.14(^{10}_{4})$ | $0.18(^{8}_{4})$ | $0.24(^{15}_{7})$ | $0.15(^{12}_{5})$ | $0.10(^{4}_{2})$ | $0.18(^{13}_{5})$ | $0.16(^{3}_{2})$ | $0.042(^{57}_{15})$ |
| data points; $\sigma_{\Theta_{\rm exp}}$ | 6 ; 1.70 | 10 ; 1.20 | 7 ; 0.72 | 5 ; 0.98 | 14 ; 0.72 **L** | 6 ; 1.20 | 47 ; 1.21 | 3 ; 0.18 **L** |
| $[\sigma_{\Theta,\rm low}, \sigma_{\Theta,\rm high}]$ [34] | [0.48,1.89] | [0.65,1.82] | [0.52,1.87] | [0.41,1.90] | [0.73,1.77] | [0.48,1.89] | [0.97,1.59] | [0.19,1.91] |
| $T_{1/2}(^{284}113)$ (s) | $1.17(^{80}_{34})$ | $1.18(^{59}_{30})$ | $1.06(^{64}_{29})$ | $1.13(^{91}_{35})$ | $0.67(^{26}_{14})$ | $0.56(^{39}_{16})$ | $0.92(^{16}_{12})$ | $0.082(^{199}_{34})$ |
| data points; $\sigma_{\Theta_{\rm exp}}$ | 6 ; 1.93 **H** | 9 ; 0.78 | 7 ; 0.78 | 5 ; 1.56 | 13 ; 0.99 | 6 ; 0.53 | 46 ; 1.17 | 2 ; 0.38 |
| $[\sigma_{\Theta,\rm low}, \sigma_{\Theta,\rm high}]$ [34] | [0.48,1.89] | [0.62,1.84] | [0.52,1.87] | [0.41,1.90] | [0.72,1.77] | [0.48,1.89] | [0.96,1.60] | [0.04,1.83] |
| $T_{1/2}(^{280}$Rg) (s) | $2.2(^{14}_{6})$ | $4.9(^{21}_{11})$ | $11.3(^{78}_{33})$ | $3.9(^{27}_{11})$ | $4.0(^{17}_{9})$ | $4.2(^{29}_{12})$ | $4.8(^{8}_{6})$ | $0.093(^{223}_{38})$ |
| data points; $\sigma_{\Theta_{\rm exp}}$ | 7 ; 0.88 | 11 ; 1.11 | 6 ; 0.40 **L** | 6 ; 0.94 | 11 ; 1.04 | 6 ; 0.84 | 47 ; 1.07 | 2 ; 1.36 |
| $[\sigma_{\Theta,\rm low}, \sigma_{\Theta,\rm high}]$ [34] | [0.52,1.87] | [0.67,1.81] | [0.48,1.89] | [0.48,1.89] | [0.67,1.81] | [0.48,1.89] | [0.97,1.59] | [0.04,1.83] |
| $T_{1/2}(^{276}$Mt) (s) | $0.90(^{55}_{25})$ | $0.53(^{26}_{13})$ | $1.48(^{120}_{46})$ | $0.29(^{29}_{10})$ | $0.42(^{18}_{10})$ | $0.90(^{73}_{28})$ | $0.70(^{13}_{9})$ | $0.021(^{28}_{8})$ |
| data points; $\sigma_{\Theta_{\rm exp}}$ | 7 ; 1.25 | 9 ; 1.14 | 5 ; 1.62 | 4 ; 1.21 | 11 ; 0.62 **L** | 5 ; 0.88 | 41 ; 1.15 | 3 ; 0.54 |
| $[\sigma_{\Theta,\rm low}, \sigma_{\Theta,\rm high}]$ [34] | [0.52,1.87] | [0.62,1.84] | [0.41,1.90] | [0.31,1.92] | [0.67,1.81] | [0.41,1.90] | [0.94,1.62] | [0.19,1.91] |
| $T_{1/2}(^{272}$Bh) (s) | $4.1(^{25}_{11})$ | $23.5(^{162}_{68})$ | $9.7(^{67}_{28})$ | $6.4(^{64}_{21})$ | $9.0(^{42}_{22})$ | $13.9(^{113}_{43})$ | $10.9(^{21}_{15})$ | $1.8(^{43}_{7})$ |
| data points; $\sigma_{\Theta_{\rm exp}}$ | 7 ; 1.51 | 6 ; 1.30 | 6 ; 0.76 | 4 ; 1.59 | 10 ; 1.12 | 5 ; 0.86 | 39 ; 1.38 | 2 ; 0.19 |
| $[\sigma_{\Theta,\rm low}, \sigma_{\Theta,\rm high}]$ [34] | [0.52,1.87] | [0.48,1.89] | [0.48,1.89] | [0.31,1.92] | [0.65,1.82] | [0.41,1.90] | [0.94,1.62] | [0.04,1.83] |
| $T_{1/2}(^{268}$Db) (h) | $23(^{14}_{6})$ | $15(^{6}_{3})$ | $22(^{12}_{6})$ | $34(^{23}_{10})$ | $28(^{10}_{6})$ | $34(^{23}_{10})$ | $25(^{4}_{3})$ | $1.4(^{18}_{5})$ |
| data points; $\sigma_{\Theta_{\rm exp}}$ | 7 ; 0.77 | 12 ; 0.83 | 8 ; 1.04 | 6 ; 0.89 | 14 ; 1.20 | 6 ; 0.73 | 53 ; 1.00 | 3 ; 0.79 |
| $[\sigma_{\Theta,\rm low}, \sigma_{\Theta,\rm high}]$ [34] | [0.52,1.87] | [0.70,1.79] | [0.58,1.85] | [0.48,1.89] | [0.73,1.77] | [0.48,1.89] | [0.98,1.58] | [0.19,1.91] |

[a] TASISpec chain measured at 245.0 MeV [5] included.

TABLE V. Half-lives derived from the correlation times of decays of isotopes of Rg, $Z = 113$ and $Z = 115$. Results and confidence intervals of a statistical test proposed in Ref. [34] are provided for each half-life analysis. The columns labeled '$4n$ channel' and '$3n$ channel' relate to the three and 53 decay chains associated with these reaction channels in Refs. [5, 9, 28], respectively. The other columns describe different combinations of the decay data from recoil-$\alpha$-SF and recoil-$\alpha$-$\alpha$-SF events detailed in Table I. This is an extended version of Table II.

| data selection | $4n$ [5, 9] | $3n$ [5, 9] | C1-C7 D1-D4 | C1-C7 D1,D2,D4 | C1-C3,C5-C7 D1,D2 | C4,D4 | C1,C2 |
|---|---|---|---|---|---|---|---|
| $T_{1/2}(Z = 115)$ (s) | $0.042(^{57}_{15})$ | $0.16(^{3}_{2})$ | $0.39(^{17}_{9})$ | $0.26(^{12}_{6})$ | $0.19(^{11}_{5})$ | $0.54(^{129}_{22})$ | $0.11(^{26}_{4})$ |
| data points; $\sigma_{\Theta_{\rm exp}}$ | 3 ; 0.18 **L** | 47 ; 1.21 | 11 ; 1.19 | 10 ; 1.02 | 8 ; 0.78 | 2 ; 1.65 | 2 ; 0.63 |
| $[\sigma_{\Theta,\rm low}, \sigma_{\Theta,\rm high}]$ [34] | [0.19,1.91] | [0.97,1.59] | [0.67,1.81] | [0.65,1.82] | [0.58,1.85] | [0.04,1.83] | [0.04,1.83] |
| $T_{1/2}(Z = 113)$ (s) | $0.082(^{199}_{34})$ | $0.92(^{16}_{12})$ | $2.0(^{9}_{5})$ | $0.63(^{29}_{15})$ | $0.75(^{41}_{20})$ | $0.17(^{42}_{7})$ | $0.35(^{85}_{15})$ |
| data points; $\sigma_{\Theta_{\rm exp}}$ | 2 ; 0.38 | 46 ; 1.17 | 11 ; 1.57 | 10 ; 1.21 | 8 ; 0.69 | 2 ; 1.44 | 2 ; 0.02 **L** |
| $[\sigma_{\Theta,\rm low}, \sigma_{\Theta,\rm high}]$ [34] | [0.04,1.83] | [0.96,1.60] | [0.67,1.81] | [0.65,1.82] | [0.58,1.85] | [0.04,1.83] | [0.04,1.83] |
| $T_{1/2}$(Rg) (s) | $0.093(^{223}_{38})$ | $4.8(^{8}_{6})$ | $7.0(^{35}_{18})$ | $2.7(^{15}_{7})$ | $3.5(^{24}_{10})$ | $0.19(^{46}_{8})$ | n/a |
| data points; $\sigma_{\Theta_{\rm exp}}$ | 2 ; 1.36 | 47 ; 1.07 0 | 9 ; 1.90 **H** | 8 ; 1.59 | 6 ; 1.18 | 2 ; 0.78 | |
| $[\sigma_{\Theta,\rm low}, \sigma_{\Theta,\rm high}]$ [34] | [0.04,1.83] | [0.97,1.59] | [0.62,1.84] | [0.58,1.85] | [0.48,1.89] | [0.04,1.83] | |

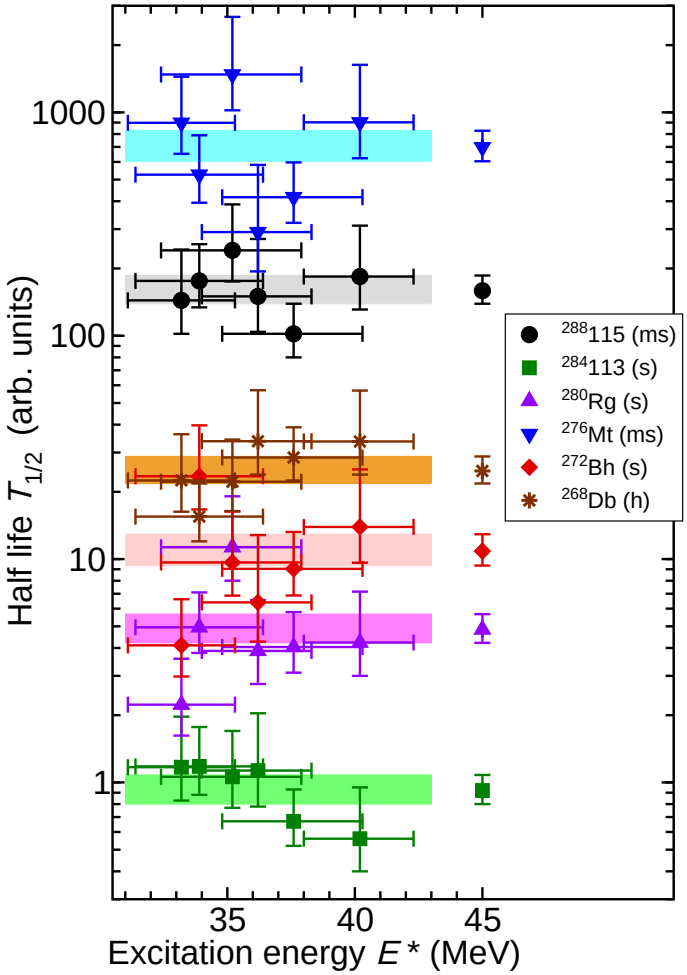



FIG. 4. (Color online) Half-life analysis for 53 decay chains associated with the production of $^{288}115$ [5, 9]. The data are split according to six different excitation energies, $E^*$, of the compound system $^{291}115$ [20]. The average is plotted on the right hand side, with its error margin represented by the shaded rectangles. See Table SM IV for details.

TABLE VI. Practical probability check of the first three decay steps of all hitherto published 67 decay chains (Refs. [5, 9] and present data set) associated with the direct production of an isotope of element $Z = 115$. For each of the decay steps, $i = 1, 2, 3$, $P_i$ is the reference probability density function for correlation times on a logarithmic scale (see Ref. [34]) evaluated for the measured correlation time. The values are normalised with the constant $e$, and given in percent. To account for the uncertainties in the reference half-lives, $P_i$ is given the value 100 % whenever the correlation time is within the confidence limits. If it is above (below) the confidence interval, the upper (lower) limit is used. $\langle P_t \rangle = \sqrt[n]{\prod P_i}$ is the geometric average. Reference values are $T_{1/2}(Z = 115) = 0.16(^{3}_{2})$ s, $T_{1/2}(Z = 113) = 0.92(^{16}_{12})$ s, and $T_{1/2}(\mathrm{Rg}) = 4.8(^{8}_{6})$ s, corresponding to the 53 five-$\alpha$-long decay chains associated with the decay of $^{288}115$ (cf. Ref. [28] and Fig. 1). Decay energies are marked '+', 'L', 'H', if the measured decay energy is compatible with the range $E_1 = [10.3, 10.6]$ MeV and $E_2 = [9.9, 10.1]$ MeV or either too low or too high, respectively. These energy ranges are defined either by full-energy measurements given in Ref. [9], and full- or reconstructed energy measurements provided in Ref. [5], cross-checked with Geant4 simulations [5, 29, 33]. 'n/a' denotes incomplete or missing data.

| chain ID | $P_1$ (%) | $P_2$ (%) | $P_3$ (%) | $\langle P_t \rangle$ (%) | $E_1$ | $E_2$ |
|---|---|---|---|---|---|---|
| Chains attributed to the $3n$ channel in Ref. [5] | | | | | | |
| 1 | 95 | 98 | 95 | 96 | + | L |
| 2 | 99 | 100 | 98 | 99 | + | + |
| 3[a] | n/a | n/a | 65 | 65 | n/a | + |
| 4 | 100 | 100 | 34 | 70 | + | + |
| 5 | 96 | 46 | 94 | 75 | + | + |
| 6 | 60 | 99 | n/a | 77 | n/a | + |
| 7 | 64 | 69 | 100 | 76 | + | + |
| 8 | 74 | 90 | 60 | 74 | n/a | + |
| 9 | 96 | 97 | n/a | 97 | + | + |
| 10 | 67 | 74 | 54 | 65 | n/a | + |
| 11 | 45 | 22 | 100 | 46 | + | + |
| 12 | 100 | 89 | 82 | 90 | + | + |
| 13[a] | 61 | 58 | 23 | 43 | n/a | + |
| 14 | 100 | 58 | n/a | 76 | + | + |
| 15 | 88 | 99 | 94 | 93 | + | + |
| 16 | 97 | 36 | 93 | 69 | + | L |
| 17 | 63 | 90 | 93 | 81 | n/a | + |
| 18 | n/a | <98 | 100 | <99 | n/a | L |
| 19 | 44 | 43 | 84 | 54 | + | + |
| 20 | 61 | 100 | 85 | 80 | + | + |
| 21 | 87 | n/a | 99 | 93 | + | n/a |
| 22 | 100 | 99 | 30 | 67 | n/a | + |
| Chains attributed to the $3n$ channel in Ref. [9] | | | | | | |
| 1 | n/a | <96 | 24 | <48 | n/a | + |
| 2 | 69 | 90 | 30 | 57 | + | + |
| 3[a] | 9.0 | 86 | 56 | 35 | + | + |
| 4 | 41 | 100 | 100 | 74 | + | + |
| 5[a] | 35 | 5.0 | 85 | 25 | + | + |
| 6[a] | 20 | 20 | 99 | 34 | + | + |
| 7[a] | 9.4 | 62 | 96 | 38 | + | + |
| 8 | 66 | 65 | 47 | 58 | + | + |
| 9[a] | 46 | 100 | 19 | 44 | + | + |
| 10 | 38 | 98 | 96 | 71 | + | + |
| 11 | n/a | <100 | 100 | <100 | n/a | + |
| 12 | n/a | <100 | 100 | <100 | n/a | + |
| 13 | 93 | 99 | 95 | 96 | + | + |
| 14[a] | 18 | 73 | 100 | 50 | + | L |
| 15[a] | 53 | 35 | 83 | 54 | + | + |
| 16 | 96 | 98 | 35 | 69 | + | + |
| 17 | 86 | 82 | 66 | 77 | + | + |
| 18 | 96 | n/a | <100 | <98 | + | n/a |
| 19 | 100 | 89 | 96 | 95 | + | + |
| 20 | 58 | 93 | 90 | 79 | + | + |
| 21[a] | 64 | 10 | 100 | 40 | + | + |
| 22 | 42 | 100 | 80 | 70 | + | + |
| 23[b] | 100 | n/a | 28 | 52 | + | + |
| 24[a] | 89 | 32 | 36 | 47 | + | + |
| 25 | n/a | <67 | 57 | <62 | n/a | + |
| 26 | 80 | 97 | 75 | 83 | + | + |
| 27 | 100 | 100 | 86 | 95 | + | + |
| 28 | 35 | 63 | 60 | 51 | + | + |
| 29 | 73 | 64 | 84 | 73 | + | + |
| 30 | 23 | 100 | 96 | 60 | + | + |
| 31 | 100 | 78 | 60 | 77 | + | + |
| Chains attributed to the $4n$ channel in Refs. [5, 9] | | | | | | |
| 1 | 65 | 15 | 0.72 | 8.9 | + | H |
| 2 | 49 | n/a | <5.4 | <16 | + | n/a |
| 3 | 50 | 31 | 11 | 25 | + | + |
| Recoil-$\alpha$-($\alpha$)-SF chains, present data and Ref. [9] | | | | | | |
| C1 | 100 | 64 | n/a | 80 | + | n/a |
| C2 | 63 | 63 | n/a | 63 | n/a | n/a |
| C3 | 100 | 100 | 15 | 53 | + | + |
| C4 | 7.0 | 6.0 | 18 | 9.2 | + | + |
| C5 | 97 | 63 | 82 | 79 | + | + |
| C6 | 100 | 100 | 100 | 100 | + | + |
| C7 | 41 | 91 | 80 | 67 | n/a | n/a |
| D1 | 100 | 100 | 64 | 86 | + | + |
| D2 | 64 | 100 | 72 | 77 | + | + |
| D3 | 0.44 | 0.0020 | 1.2 | 0.10 | + | L |
| D4 | 55 | 73 | 4.0 | 25 | + | H |

[a] Chain assignment relies also on decay energies and correlation times of subsequent decay steps [30].
[b] The long-lived $\alpha$ decay assigned to $^{276}$Mt in Ref. [9] is associated with $^{280}$Rg [5].

TABLE VII. Similar to Table SM VI but using the average of the eleven recoil-$\alpha$(-$\alpha$)-SF chains C1-C7 and D1-D4 as reference. Reference values are $T_{1/2}(Z = 115) = 0.39(^{17}_{9})$ s, $T_{1/2}(Z = 113) = 2.0(^{9}_{5})$ s, and $T_{1/2}(\mathrm{Rg}) = 7.0(^{35}_{18})$ s (cf. column 2 in Table II or column 3 in Table V). Energy ranges are $E_1 = [10.3, 10.6]$ MeV and $E_2 = [9.5, 10.2]$ MeV.

| chain ID | $P_1$ (%) | $P_2$ (%) | $P_3$ (%) | $\langle P_t \rangle$ (%) | $E_1$ | $E_2$ |
|---|---|---|---|---|---|---|
| Recoil-$\alpha$-SF chains, present data and Ref. [9] | | | | | | |
| C1 | 84 | 40 | n/a | 58 | + | n/a |
| C2 | 35 | 39 | n/a | 37 | n/a | n/a |
| C3 | 90 | 85 | 12 | 45 | + | + |
| C4 | 81 | 3.3 | 15 | 16 | + | + |
| C5 | 98 | 39 | 100 | 73 | + | + |
| C6 | 81 | 81 | 100 | 87 | + | + |
| C7 | 100 | 100 | 71 | 89 | n/a | n/a |
| D1 | 89 | 92 | 55 | 77 | + | + |
| D2 | 36 | 95 | 63 | 60 | + | + |
| D3 | 43 | 6.6 | 20 | 18 | + | + |
| D4 | 30 | 47 | 3.3 | 17 | + | + |
| $\langle$FoM$\rangle$ | | | | **52** | | |

TABLE VIII. Similar to Table SM VII but isolating chain D3. This corresponds to 'scenario 1' illustrated in Fig. 2(a). Reference values are $T_{1/2}(Z = 115) = 0.26(^{12}_{6})$ s, $T_{1/2}(Z = 113) = 0.63(^{29}_{15})$ s, and $T_{1/2}(\mathrm{Rg}) = 2.7(^{15}_{7})$ s (cf. column 3 in Table II or column 5 in Table V). Energy ranges are $E_1 = [10.3, 10.6]$ MeV and $E_2 = [9.9, 10.2]$ MeV.

| chain ID | $P_1$ (%) | $P_2$ (%) | $P_3$ (%) | $\langle P_t \rangle$ (%) | $E_1$ | $E_2$ |
|---|---|---|---|---|---|---|
| Recoil-$\alpha$-($\alpha$)-SF chains, present data and Ref. [9] | | | | | | |
| C1 | 97 | 86 | n/a | 91 | + | n/a |
| C2 | 49 | 85 | n/a | 64 | n/a | n/a |
| C3 | 100 | 100 | 12 | 49 | + | + |
| C4 | 50 | 9.9 | 15 | 19 | + | + |
| C5 | 100 | 85 | 60 | 80 | + | + |
| C6 | 96 | 100 | 95 | 97 | + | + |
| C7 | 91 | 82 | 71 | 81 | n/a | n/a |
| D1 | 99 | 100 | 55 | 82 | + | + |
| D2 | 50 | 99 | 63 | 67 | + | + |
| D4 | 42 | 93 | 3.3 | 23 | + | + |
| $\langle$FoM$\rangle$ | | | | **65** | | |
| D3 | 16 | 0.0002 | 0.13 | 0.074 | + | L |

TABLE IX. Similar to Table SM VII but assuming that ten recoil-$\alpha$-($\alpha$)-SF chains (not D3) have the same origin as the 53 five-$\alpha$-long chains [5, 9]. This corresponds to 'scenario 2' illustrated in Fig. 2(b). Reference values are $T_{1/2}(Z = 115) = 0.18(^{5}_{2})$ s, $T_{1/2}(Z = 113) = 0.87(^{13}_{10})$ s, and $T_{1/2}(\mathrm{Rg}) = 4.5(^{7}_{5})$ s [cf. Fig. 2(b)]. Energy ranges are $E_1 = [10.3, 10.6]$ MeV and $E_2 = [9.9, 10.1]$ MeV.

| chain ID | $P_1$ (%) | $P_2$ (%) | $P_3$ (%) | $\langle P_t \rangle$ (%) | $E_1$ | $E_2$ |
|---|---|---|---|---|---|---|
| Recoil-$\alpha$-($\alpha$)-SF chains, present data and Ref. [9] | | | | | | |
| C1 | 100 | 66 | n/a | 81 | + | n/a |
| C2 | 57 | 64 | n/a | 61 | n/a | n/a |
| C3 | 100 | 100 | 15 | 53 | + | + |
| C4 | 11 | 6.3 | 19 | 11 | + | + |
| C5 | 99 | 65 | 77 | 79 | + | + |
| C6 | 100 | 100 | 100 | 100 | + | + |
| C7 | 50 | 87 | 83 | 71 | n/a | n/a |
| D1 | 100 | 100 | 66 | 87 | + | + |
| D2 | 58 | 100 | 74 | 76 | + | + |
| D4 | 50 | 75 | 4.2 | 25 | + | H |
| $\langle$FoM$\rangle$ | | | | **64** | | |
| D3 | 0.90 | 0.0007 | 0.72 | 0.076 | + | L |

TABLE X. Similar to Table SM IX but associating chains C4 and D4 with a separate origin of decay. This corresponds to the (preferred) 'scenario 3' illustrated in Fig. 2(c). Reference values for these two chains C4 and D4 are $T_{1/2}(Z = 115) = 0.54(^{129}_{22})$ s, $T_{1/2}(Z = 113) = 0.17(^{42}_{7})$ s, $T_{1/2}(\mathrm{Rg}) = 0.19(^{46}_{8})$ s (cf. column 5 in Table II or column 6 in Table V), $E_1 = [10.3, 10.6]$ MeV, and $E_2 = [9.9, 10.2]$ MeV. Reference values for the remaining eight recoil-$\alpha$-($\alpha$)-SF chains are $T_{1/2}(Z = 115) = 0.16(^{3}_{2})$ s, $T_{1/2}(Z = 113) = 0.90(^{14}_{11})$ s, $T_{1/2}(\mathrm{Rg}) = 4.7(^{7}_{6})$ s [cf. Fig. 2(c)], $E_1 = [10.3, 10.6]$ MeV, and $E_2 = [9.9, 10.1]$ MeV by attributing these to the same decay origin as 53 five-$\alpha$-long chains [5, 9].

| chain ID | $P_1$ (%) | $P_2$ (%) | $P_3$ (%) | $\langle P_t \rangle$ (%) | $E_1$ | $E_2$ |
|---|---|---|---|---|---|---|
| Recoil-$\alpha$-($\alpha$)-SF chains, present data and Ref. [9] | | | | | | |
| C1 | 100 | 65 | n/a | 80 | + | n/a |
| C2 | 63 | 63 | n/a | 63 | n/a | n/a |
| C3 | 100 | 100 | 15 | 53 | + | + |
| C5 | 97 | 64 | 79 | 79 | + | + |
| C6 | 100 | 100 | 100 | 100 | + | + |
| C7 | 41 | 89 | 81 | 67 | n/a | n/a |
| D1 | 100 | 100 | 65 | 87 | + | + |
| D2 | 64 | 100 | 73 | 78 | + | + |
| C4 | 100 | 41 | 100 | 74 | + | + |
| D4 | 28 | 100 | 88 | 63 | + | + |
| $\langle$FoM$\rangle$ | | | | **74** | | |

[1] R.C. Barber, P.J. Karol, H. Nakahara, E. Vardaci, and E. Vogt, Pure Appl. Chem. **83** (7), 1485 (2011).
[2] A. Bohr and B.R. Mottelson, *Nuclear Structure Volume II*, (W. A. Benjamin, Inc., Massachusetts, 1975).
[3] G.T. Seaborg and W.D. Loveland, *The Elements Beyond Uranium*, (Wiley-Interscience, New York, 1990).
[4] R.-D. Herzberg and P.T. Greenlees, Prog. Part. Nucl. Phys. **61**, 674 (2008).
[5] D. Rudolph *et al.*, Phys. Rev. Lett. **111**, 112502 (2013).
[6] Yu. Ts. Oganessian *et al.*, Phys. Rev. Lett. **104**, 142502 (2010).
[7] Yu. Ts. Oganessian, Radiochim. Acta **99**, 429 (2011).
[8] Yu. Ts. Oganessian *et al.*, Phys. Rev. Lett. **108**, 022502 (2012).
[9] Yu. Ts. Oganessian *et al.*, Phys. Rev. C **87**, 014302 (2013).
[10] Yu. Ts. Oganessian *et al.*, Phys. Rev. C **87**, 054621 (2013).
[11] J. Khuyagbaatar *et al.*, Phys. Rev. Lett. **112**, 172501 (2014).
[12] K. Morita *et al.*, J. Phys. Soc. Jpn. **81** 103201 (2012).
[13] Yu. Ts. Oganessian *et al.*, Phys. Rev. C **69**, 021601(R) (2004).
[14] M. Schädel, Eur. Phys. J. D **45**, 67 (2007).
[15] A. Semchenkov *et al.*, Nucl. Instr. Meth. **B266**, 4153 (2008).
[16] J.M. Gates *et al.*, Phys. Rev. C **83**, 054618 (2011).
[17] E. Jäger, Ch.E. Düllmann, J. Khuyagbaatar, J. Krier, M. Schädel, T. Torres, and A. Yakushev, J. Radioanal. Nucl. Chem. **299**, 1073 (2014).
[18] J. Runke *et al.*, J. Radioanal. Nucl. Chem. **299**, 1081 (2014).
[19] J.F. Ziegler, Nucl. Instr. Meth. **A219**, 1024 (2004).
[20] W.D. Myers and W.J. Swiatecki, Nucl. Phys. **A601**, 141 (1996).
[21] J. Khuyagbaatar *et al.*, Nucl. Instr. Meth. **A689**, 40 (2012).
[22] U. Forsberg *et al.*, Acta Phys. Pol. **43**, 305 (2012).
[23] L.-L. Andersson *et al.*, Nucl. Instr. Meth. **A622**, 164 (2010).
[24] K.E. Gregorich, Nucl. Instr. Meth. **A711**, 47 (2013).
[25] P. Golubev *et al.*, Nucl. Instrum. Meth. **A723**, 55 (2013).
[26] J. Hoffmann *et al.*, GSI Scientific Report 2011, GSI Report 2012-1 (2012).
[27] U. Forsberg *et al.*, Eur. Phys. J. Web of Conferences **66**, 02036 (2014).
[28] D. Rudolph *et al.*, Acta Phys. Pol. **B45**, 263 (2014).
[29] D. Rudolph *et al.*, J. Rad. Nucl. Chem., (2014) DOI 10.1007/s10967-014-3445-y .
[30] U. Forsberg *et al.*, to be published.
[31] See Supplemental Material at http://link.aps.org .
[32] L.G. Sarmiento, L.-L. Andersson, D. Rudolph, Nucl. Instr. Meth. **A667**, 26 (2012).
[33] L.G. Sarmiento *et al.*, Proc. 10th Latin American Symposium on Nuclear Physics and Applications, PoS(X LASNPA)057 (2014).
[34] K.-H. Schmidt, Eur. Phys. J. A **8**, 141 (2000).
[35] Yu. Ts. Oganessian *et al.*, Phys. Rev. C **83**, 054315 (2011).
[36] K.-H. Schmidt, C.-C. Sahm, K. Pielenz, and H.-G. Clerc, Z. Phys. A **316**, 19 (1984).
[37] V.I. Zagrebaev, Nucl. Phys. **A734**, 164 (2004).
[38] K. Siwek-Wilczyńska, T. Cap, M. Kowal, A. Sobiczewski, and J. Wilczyński, Phys. Rev. C **86**, 014611 (2012).
[39] W. Reisdorf and M. Schädel, Z. Phys. A **343**, 47 (1992).
[40] Ch.E. Düllmann *et al.*, Phys. Rev. Lett. **104**, 252701 (2010).
[41] R. Smolańczuk, J. Skalski and A. Sobiczewski, Phys. Rev. C **52**, 1871 (1995).
[42] M. Warda and J.L. Egido, Phys. Rev. C **86**, 014322 (2012).
[43] A. Staszczak, A. Baran, and W. Nazarewicz, Phys. Rev. C **87**, 024320 (2013).
[44] D.C. Hoffman and M.R. Lane, Radiochim. Acta **70/71**, 135 (1995).
[45] F.P. Heßberger, Eur. Phys. J. Web of Conferences **66**, 02048 (2014).
[46] A.V. Karpov, V.I. Zagrebaev, Y. Martinez Palenzuela, L. Felipe Ruiz, and W. Greiner, Int. J. Mod. Phys. **E21**, 1250013 (2012).
[47] V. Zagrebaev, A. Karpov, and W. Greiner, J. Phys.: Conf. Ser. **420**, 012001 (2013); Acta Phys. Pol. **45**, 291 (2014).
[48] B.G. Carlsson and I. Ragnarsson, Phys. Rev. C **74**, 011302 (2006).
[49] S.G. Nilsson, C.F. Tsang, A. Sobiczewski, Z. Szymański, S. Wycech, C. Gustafson, I.-L. Lamm, P. Möller, and B. Nilsson, Nucl. Phys. A **131**, 1 (1969).
[50] A. Parkhomenko and A. Sobiczewski, Acta Phys. Pol. **B35**, 2447 (2004).
[51] S. Ćwiok, W. Nazarewicz, and P.H. Heenen, Phys. Rev. Lett. **83**, 1108 (1999).
[52] M. Kortelainen, J. McDonnell, W. Nazarewicz, P.-G. Reinhard, J. Sarich, N. Schunck, M.V. Stoitsov, and S.M. Wild, Phys. Rev. C **85**, 024304 (2012).
[53] Yue Shi, D.E. Ward, B.G. Carlsson, J. Dobaczewski, W. Nazarewicz, I. Ragnarsson, and D. Rudolph, Phys. Rev. C **90**, 014308 (2014).